Self-Assembled Curved Macroporous Photonic Crystal-Based Surfactant Detectors

Chien-Fu Chiu,[†] Hui-Ping Tsai,[‡] Ying-Chu Chen,[†] Yi-Xuan He,[†] Kun-Yi Andrew Lin,*,[§] and Hongta Yang*,[†]

[†]Department of Chemical Engineering, [‡]Department of Civil Engineering, and [§]Department of Environmental Engineering, National Chung Hsing University, 250 Kuo-Kuang Rd., Taichung 402, Taiwan

S *Supporting Information*

ABSTRACT: Surfactants are extensively used as detergents, dispersants, and emulsifiers. Thus, wastewater containing high-concentration surfactants discharged to the environment pose a serious threat to the ecosystem. Unfortunately, conventional detection methods for surfactants suffer from the use of sophisticated instruments and cannot perform detections for various surfactants by a single analysis. The article reports the development of simple and sensitive surfactant detection using doctor-blade-coated three-dimensional curved macroporous photonic crystals on a cylindrical rod. The photonic crystals exhibit different hydrophobicities at various angular positions after surface modification. The penetration of aqueous surfactant solutions in the interconnected macropores causes red-shift as well as reduction in amplitude in the optical stop bands, resulting in surfactant detection with visible readout. The correlation between the surface tension, as well as the solution-infiltrated angular position, and the concentration of aqueous surfactant solutions has also been investigated in this study.

KEYWORDS: self-assembly, photonic crystals, hydrophobicity, doctor blade coating, surfactant detection
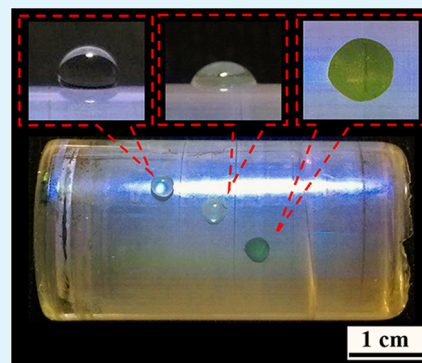
1. INTRODUCTION

Surfactants, consisting of both hydrophilic and lipophilic moieties, are compounds that reduce the interfacial tension between two phases, making them widely used in household, industrial, agricultural, and pharmaceutical products as diverse as detergents, dispersants, emulsifiers, petroleum products, pesticides, and cosmetics.[1−3] Recently, concerns about ecotoxicity of surfactants arise from extensive usage of surfactants and the resulting effects caused by their disposal to the environment, which seriously inhibit the growth of aquatic organisms and inevitably pose risks to various aspects of the ecosystem.[4] In addition, bioaccumulation of surfactants through food chains and potable water arouses reduction in the activity of various enzymes in the human body, resulting in pathological changes.[5,6] To address the environmental issues and reduce the increasing chemosensory irritations in humans, it is imperative to regulate and monitor the concentration of surfactants discharged to sewage and aquatic environment.[7] Therefore, there is an urgent demand for rapid and convenient analysis of surfactant concentrations.

To date, several methods have been developed for the analysis of surfactants, such as gas and liquid chromatography, refractometric analysis, capillary electrophoresis, charged aerosol analysis, light-scattering measurement, mass spectrometry, and fluorescence techniques.[8−14] However, most of the existing technologies have serious issues, such as low sensitivity, high cost and sophisticated instrumentation, and time-consuming analysis, making them difficult for rapid detection.[15]

Moreover, typical approaches cannot be used to detect different types of surfactants in a single analysis.[16] Therefore, it is highly desired to develop a universal methodology, rendering it suitable for surfactant detection when pursuing exploratory research.

Photonic crystals (also called photonic band gap materials) consist of periodic dielectric structures with gaps for electromagnetic waves.[17,18] Exemplified by blue *Morpho* butterfly wing scales, three-dimensional photonic crystals are readily available for exploring interesting ideas and materials through adjustable colors in the past few decades.[19,20] Through the variation of optical characteristics, including wavelength shift of photonic band gaps as well as the Fabry−Perot fringes of diffractive media, the concentration of chemicals can be deduced.[21−25] The photonic crystal-based chemical sensors exhibit several advantages over other sensing methods in immunity to electromagnetic interface, portability, short response time, online monitoring capability, and stability.[26,27] Mould-shaping technologies have been widely applied to pattern photonic crystals.[28] Unfortunately, the most rigid moulds at nanometer-scale dimensions are brittle and expensive to prepare, whereas the feature sizes of elastomeric moulds are limited to submicrometer-scale dimensions.[29] Additionally, the methodology is only capable of developing photonic crystals with a few

structural layer thickness and required to generate new moulds for different patterns.[30] Recently, the preparation of photonic crystals using top-down or bottom-up approaches has been demonstrated. For instance, spherical colloids dispersed in a monomer crystallize into non-close-packed face-centered cubic configurations spontaneously under the influence of van der Waals attractions and electrostatic interactions between colloids.[31,32] This method, in comparison with traditional lithography-based fabrication technologies, provides a convenient and low-cost approach for creating photonic crystals.[21−33] Nevertheless, the existing techniques of self-assembled colloidal methodologies, including gravity sedimentation, dip-coating, spin-coating, capillary force-induced self-assembly, evaporation-induced convective assembly, and electric-field-assisted self-assembly, exhibit technical incompatibility with mature micro-fabrication and are merely feasible for laboratory-scale fabrication.[34−40]

For scaling up production, a roll-to-roll doctor-blade-coating technology via unidirectional shear aligning colloidal suspensions has recently been developed to produce highly ordered colloidal crystal−polymer composites. After selectively removing colloidal crystals in the composite, the resulting three-dimensional macroporous polymeric photonic crystals display uniform diffractive colors.[41,42] Unfortunately, the developments of photonic crystal-based sensors are significantly impeded by the inferior chemical adsorption abilities, and thus, the sensitivity of surfactant sensing is restricted.[43] Although distinct chemical indicators are applied to offer different responding properties in the photonic crystals, most of the displacement assays are time-consuming, relatively complex, and merely used once or for a short period of time.[44,45]

In view of the inherent hydrophobicity of air, porous structures composed of a high volume of entrapped air can be manipulated to alter the surface wettability. Inspired by lotus leaves, the surface hydrophobicity of macroporous photonic crystals can be adjusted through different reactive ion etching durations, followed by a surface functionalization treatment.[46,47] It is worth mentioning that surfactants lower the surface tension of aqueous solutions through disturbing the arranged configurations of water molecules at the interface as well as diminishing the attraction between them. Therefore, an increase in the surfactant concentration of an aqueous solution lowers surface tension of the surfactant solution until the critical micelle concentration is reached.[48,49] As surfactants saturate liquid−solid interfaces, the surfactants reduce inter-facial tension of the solutions and facilitate adhesion of the solutions to solid substrates, resulting in lower contact angles or penetration of the solutions into hydrophobic porous substrates.[50] In other words, aqueous surfactant solutions with higher surfactant concentrations can spontaneously penetrate into porous media with higher hydrophobicity.

Owing to the intrinsic surface activity of surfactants, a novel technique that allows effective surfactant sensing using doctor-blade-coated curved macroporous photonic crystals, which exhibit different hydrophobicities at various angular positions, has been developed. The aqueous surfactant solutions with different surfactant concentrations infiltrate the macroporous photonic crystals with different hydrophobicities, causing a relatively high effective refractive index of diffractive media. The resultant infiltration therefore leads to color changes at different angular positions. Most importantly, the as-prepared surfactant detectors featuring a highly visible readout are portable, inexpensive, fast responsive, and suitable for various surfactants.

2. EXPERIMENTAL SECTION

2.1. Materials and Substrates. Reagents and solvents for preparing silica microspheres, including tetraethyl orthosilicate (TEOS), ammonium hydroxide (NH$_4$OH), and absolute ethanol, were provided by Sigma-Aldrich. Deionized water (18.2 MΩ cm) was obtained by a water purification system (Millipore). UV-curable ethoxylated trimethylolpropane triacrylate (ETPTA) monomer and photoinitiator, 2-hydroxy-2-methyl-1-phenyl-1-propanone (Darocur 1173), were obtained from Sartomer and Ciba-Geigy, respectively. (Tridecafluoro-1,1,2,2,-tetrahydrooctyl)-trichlorosilane employed as a modifier was received from Alfa Aesar. The surfactants, sodium dodecyl sulfate (SDS, 99%) and cetyltrimethylammonium bromide (CTAB, 99%), used in the study were acquired commercially from Sigma-Aldrich. All reagents were used without further purification. Polyacrylate cylindrical rods (2 cm in diameter and 1 cm in diameter, Bridgeacry Corporation) were used as coating substrates, which were washed repeatedly with water and then dried at ambient temperature before use.

2.2. Preparation of Silica Colloidal Suspensions. Silica microspheres with 255 nm in diameter were prepared based on the Stöber method.[51] In the synthesis process, TEOS was hydrolyzed to form silica microspheres in a mixture of absolute ethanol, deionized water, and NH$_4$OH at 25 °C for 24 h. The resulting silica microspheres were purified using absolute ethanol via cyclic centrifugation−redispersion procedures to remove impurities (i.e., NH$_4$OH, deionized water, and residual TEOS). After purification, silica microspheres (7.4 mL) were then dispersed in UV-curable ETPTA monomer (2.6 mL) with 1 vol % photoinitiator to reach a silica microsphere volume of 74 vol % using a Thermolyne vortex mixer. After filtering through a 5 μm syringe membrane for removing silica microsphere agglomeration, the transparent silica colloidal suspensions were preserved in an uncovered container for 12 h to evaporate ethanol.

2.3. Fabrication of Curved Colloidal Crystals. Three-dimensional curved silica colloidal crystals were fabricated by a scalable doctor-blade-coating technology. In the assembly procedure, a doctor blade was posed vertically on a polyacrylate cylindrical rod. The as-prepared silica colloidal suspension was distributed along a single sidewall of the blade onto the cylindrical rod. The rod was then rolled at a pre-set speed to move the colloidal suspension across the gap between the blade and the rod, while the blade could spread the suspension uniformly on the rod and offer a one-dimensional shear force to align the silica colloids that pass through the gap between the blade and the rod. After coating, ETPTA was photopolymerized rapidly to create a curved silica colloidal crystal−polymer composite by exposure to ultraviolet radiation using 40 W UV lamp. In the doctor-blade-coating procedure, various colloidal sizes ranging from 200 to 560 nm can be used to develop silica colloidal crystal−polymer composites.[41]

2.4. Preparation of Curved Macroporous Photonic Crystals. A reactive ion etcher operating at 40 mTorr, 40 sccm of argon, and 40 W was employed to etch the polymer matrix for partially exhibiting the embedded top-layer silica microspheres. To create macroporous photonic crystals, the embedded silica colloid crystals were then eliminated through dropping a 1 vol % hydrogen fluoride aqueous solution on the composite for 20 s, followed by cleaning it in absolute ethanol. The above-mentioned protocols were repeated for several cycles until the cylindrical rod became transparent in ethanol.

2.5. Surface Modification of Curved Macroporous Photonic Crystals. The hydrophobicity of the macroporous photonic crystals could be improved through surface functionalizing with fluorinated silane through chemical vapor deposition. The cylindrical rod was put into an oven, on the bottom of which was dispensed an uncovered beaker within a relatively low volume of (tridecafluoro-1,1,2,2,-tetrahydrooctyl)-trichlorosilane. Subsequently, the oven was heated up to 120 °C to evaporate the fluorinated silane. After 2 h, the rod was moved to another clean sealed chamber and pumped to volatilize the unreacted fluorinated silane molecules absorbed on the surface.
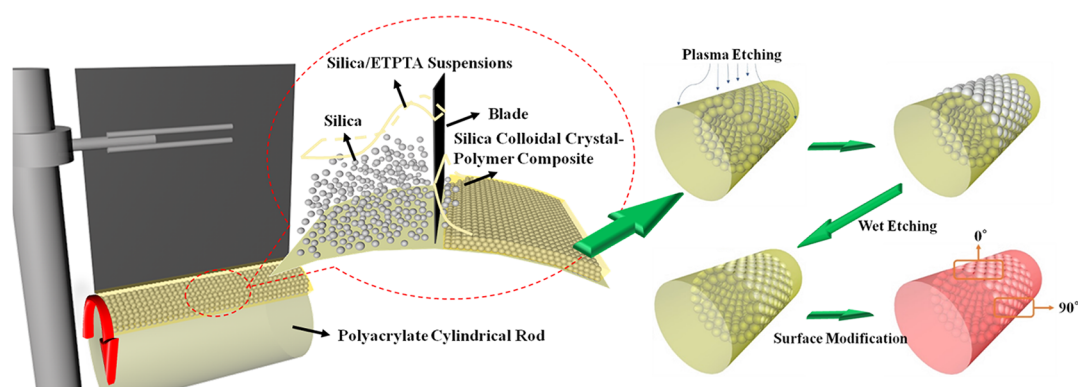
Figure 1. Schematic illustration of the experimental procedures for preparing curved macroporous photonic crystals with different hydrophobicities.

2.6. Characterization. Field-emission scanning electron microscopy (FESEM) (JEOL 6335F) was performed. Reflection spectra perpendicular to curved macroporous photonic crystal surfaces were collected by a high-resolution fiber-optic UV−visible−near-infrared (NIR) spectrometer (Ocean Optics HR4000) with Ocean Optics DT-MINI-2-B as a light source. The spectra were recorded using Ocean Optics Spectra Suite Spectroscopy Software in the wavelength ranging from 300 to 800 nm, and the cone angle of collection was smaller than 5°. Absolute reflectivity was collected as the ratio of the specimen spectrum over a reference spectrum from an aluminum-coated silicon wafer. A sessile drop-shape analysis system (KRÜSS G10) with the DropSnake imaging system was employed to acquire static water contact angles (SWCAs) of the specimens. Using an autopipetting system, a drop of 10 μL deionized water was dispensed onto the specimen surface. After raising the micropipette tip, an image of the water drop was taken. An analysis of each image results in a left and right contact angle. This process was repeated seven times on different regions for each specimen, producing 14 angle measurements per specimen. The average of these measurements was reported as the SWCA. The image of the specimen was recorded by a digital camera (Nikon COOLPIX L810).

3. RESULTS AND DISCUSSION

The scheme of the experimental protocol for preparing curved macroporous photonic crystals with different hydrophobicities is presented in Figure 1. Three-dimensional curved silica colloidal crystal−polymer composites are assembled on the surface of polyacrylate cylindrical rods by a doctor-blade-coating technique, which aligns concentrated silica colloidal suspensions. This technology allows scalable fabrication of hexagonally ordered close-packed colloidal crystals with a large-scale domain.[42] The doctor-blade-coated curved colloidal crystal−polymer composite is then transferred to a reactive ion etcher and etched by applying argon plasma etching to release the top-layer silica microspheres. Because of the high selectivity of plasma etching between silica and ETPTA polymer under above reactive ion etching conditions, the long-range arrangement of silica microspheres can be well-retained.[41] The templating silica microspheres are then wet-etched using hydrofluoric acid aqueous solution to fabricate curved macroporous photonic crystals on cylindrical rods. The resulting macroporous photonic crystals are finally functionalized by exposure to a vapor of (tridecafluoro-1,1,2,2,-tetrahydrooctyl)-trichlorosilane with low surface energy to improve the surface hydrophobicity. The silane coupling agents are hydrolyzed with moisture to result in reactive silanolic hydroxyl groups and further condense with other fluorinated silanes on the surface of macroporous photonic crystals.[52]

A top-view SEM image of the doctor-blade-coated curved macroporous photonic crystals templated from 255 nm silica microspheres is displayed in Figure 2a. The crystalline ordering of air cavities is evident, indicating that the polymer matrix does not collapse during the wet etching treatment. In comparison
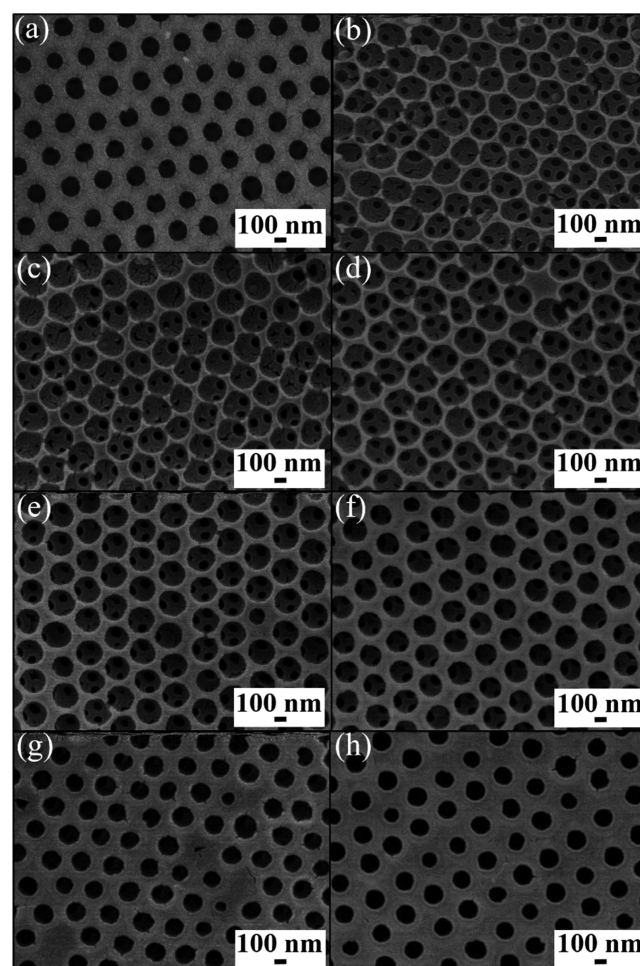

Figure 2. (a) Top-view SEM image of curved macroporous photonic crystals templated from 255 nm silica microspheres. (b−h) Top-view SEM images of the curved macroporous photonic crystals fabricated by plasma etching a silica colloidal crystal−polymer composite for 1 min, followed by selective removal of the templating silica microspheres at (b) 0°, (c) 15°, (d) 30°, (e) 45°, (f) 60°, (g) 75°, and (h) 90°.
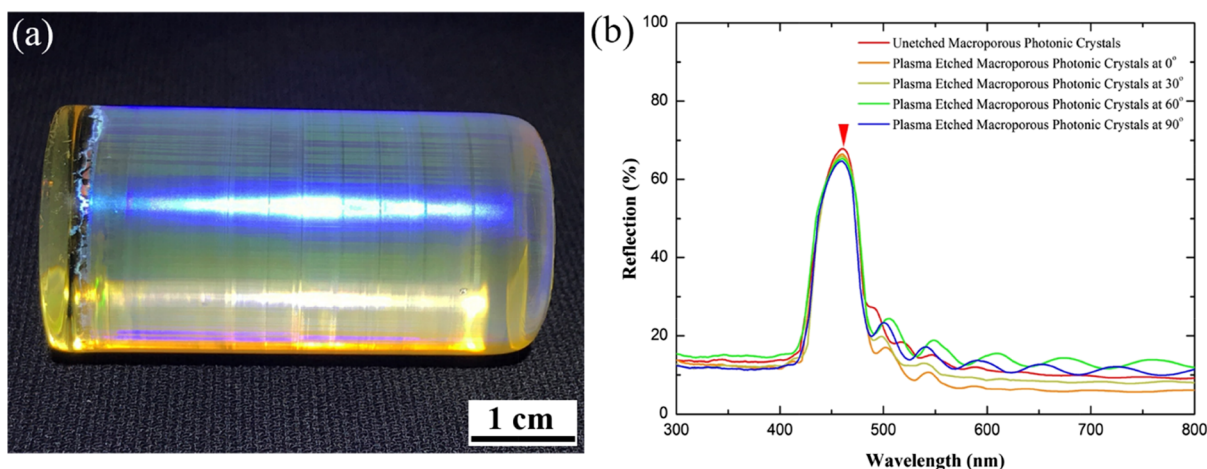
Figure 3. (a) Photograph of curved macroporous photonic crystals templated from 255 nm silica microspheres after a 1 min plasma-etching treatment. (b) Reflection spectra obtained from unetched curved macroporous photonic crystals and the curved macroporous photonic crystals after a plasma etching treatment at various angular positions.

with that, the surface morphologies of the plasma-etched curved macroporous photonic crystals at various angular positions are shown in Figure 2b−h. The macroporous photonic crystals are prepared by argon plasma etching a doctor-blade-coated curved composite at 40 mTorr, 40 sccm of argon, and 40 W for 1 min, followed by wet etching the templated 255 nm silica microspheres. The voids are interconnected through smaller pores that appear owing to the touching sites of silica microspheres in the doctor-blade-coated composite, conforming that the hexagonal ordering of close-packed silica colloidal crystals are confined in the polymer matrix. Some smaller pores blocked by the ETPTA polymer form primarily owing to the existence of silica microspheres with extreme sizes. As shown in Figure S1, it is also evident that the top hemisphere of top-layer silica microspheres can almost be exposed after argon plasma etching for 1 min at 0°, resulting in an average void size of 236 ± 4 nm (Figure 2b), which is comparable with the diameter of templating silica microspheres. Interestingly, the top-layer void size of the plasma-etched curved macroporous photonic crystals decreases as the angular position increases from 0° to 90°. Besides, the void size of the etched curved photonic crystal at 90° (Figure 2h) is approximately equal to that of unetched curved photonic crystals. It is worth noting that argon plasma proceeding in a vertical direction enables the implementation of anisotropic etching. In this system, argon gas is used for physically bombarding the composite, and the etching rate of the polymer matrix is proportional to the projected surface area perpendicular to the etching direction (Figure 1).[53] Therefore, the etching rate decreases with increasing angular position, and consequently, the void size gradually changes with different angular positions (Figure S2).

A photograph of the plasma-etched curved macroporous photonic crystals templated from 255 nm silica microspheres is displayed in Figure 3a. The curved macroporous photonic crystals exhibit a striking blue color illumined with white light, derived from Bragg diffraction of incident visible light from long-range hexagonal ordering of air cavities. This indicates that large-scale curved macroporous photonic crystals with three-dimensional crystalline arrays of pores can be created. To further comprehend the optical properties of the plasma-etched curved macroporous photonic crystals, a UV−vis−NIR

spectrometer is used to evaluate the optical reflection spectra perpendicular to the surface of curved macroporous photonic crystals at various angular positions. As shown in Figure 3b, the diffraction peak of unetched curved macroporous photonic crystals is located at 458 nm with high reflection amplitude, resulting from the high refractive index in contrast to the polymer matrix and air cavities. The position of the diffraction peak can be theoretically estimated using Bragg's law[54]

$$\lambda_{peak} = 2n_{eff} d \sin \theta$$

where n_{eff} is the effective refractive index of the medium, d denotes the interlayer spacing, and $\sin \theta$ equals to 1 at normal incidence. The calculated diffraction peak position as presented by the incident arrow is located at 460 nm, agreeing well with the experimental result. Compared with that, the shifts of the peak position for the plasma-etched curved macroporous photonic crystals are less than 1 nm at various angular positions, disclosing that the high crystalline quality of air cavities is not affected by top-layer void size after plasma etching treatments. This further demonstrates that the curved macroporous photonic crystals with different top-layer void sizes at various angular positions can be obtained. In addition, curved macroporous photonic crystals can be doctor-blade coated on the surfaces of cylindrical rods with different diameters. Figure S3 presents an image and reflection spectrum of coated curved macroporous photonic crystals templated from 255 nm silica microspheres on a rod with diameter of 1 cm. The blue color and diffraction peak position of the as-prepared photonic crystals are apparently similar to that as shown in Figure 3.

The surface of the plasma-etched curved macroporous photonic crystals can be functionalized with fluorosilane through silane coupling reaction to improve the surface hydrophobicity. As displayed in Figure 4a, the SWCA on surface-modified curved macroporous photonic crystals without plasma etching treatment is 123 ± 3°. In comparison with that, an SWCA of 151 ± 2° on surface-modified plasma-etched curved macroporous photonic crystals can be achieved at 0° (Figure 4b). Additionally, it is found that the SWCA becomes smaller when the angular position increases (Figure 4b−h), and the SWCA reaches 124 ± 2° at 90°, which is close to the
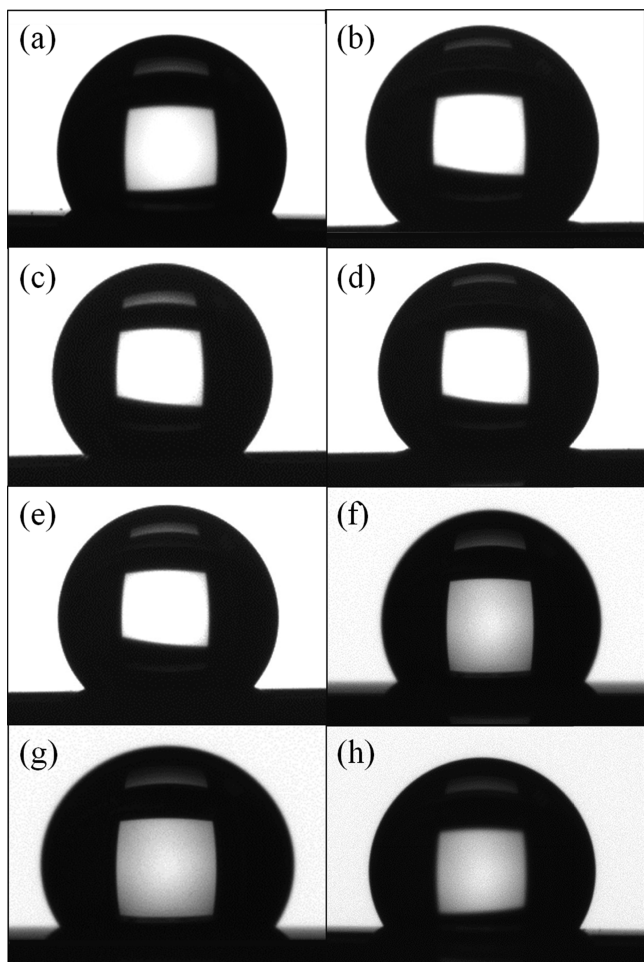
Figure 4. (a) Water drop profile on fluorosilane-modified curved macroporous photonic crystals templated from 255 nm silica microspheres. (b−h) Water drop profiles on fluorosilane-modified curved macroporous photonic crystals after a 1 min plasma-etching treatment at (b) 0°, (c) 15°, (d) 30°, (e) 45°, (f) 60°, (g) 75°, and (h) 90°.

measured SWCA on surface-modified unetched curved macroporous photonic crystals.

The surface-modified curved macroporous photonic crystal surfaces retain shining blue color when water drops wet the surfaces consisting of polymer and entrapped air. The observed incomplete wetting is therefore quantitatively explained using Cassie's model

$$\cos \theta' = f \cos \theta - (1 - f)$$

where θ' is the SWCA on a rough surface, θ is the intrinsic SWCA on a flat surface, and f is the area fraction of the polymer matrix in direct contact with a water droplet. The solid projected area fraction value, f, can be estimated by applying a trigonometric calculation as

$$f = 1 - \left(\frac{\pi R_v^2}{2\sqrt{3}\, R_s^2} \right)$$

where R_v is the radius of top-layer voids determined by averaging 100 voids in the SEM images of Figure 2 and R_s is the radius of the templating 255 nm silica microspheres. As summarized in Figure 5a, the void size decreases with the increase of the angular position, whereas the solid projected area fraction (f) value increases with the angular position. The calculated water contact angles using Cassie's model are compared with the acquired SWCAs in Figure 5b. It is apparent that the tendencies of calculated results and experimental data are similar, indicating that the entrapped air between functionalized polymer matrixes can prevent water drops from penetrating into the top-layer voids, and the Cassie's model is therefore valid for the as-created macroporous photonic crystals.

It is evident that curved macroporous photonic crystals with different surface hydrophobicities at various angular positions can be fabricated by the scalable doctor-blade-coating methodology. This unique combination provides a platform for sensing chemicals with different surface tensions. This study further evaluates the sensing characteristics by depositing 10 μL aqueous solution drops with different concentrations of SDS, which is a common anionic surfactant present in cleaning and hygiene products, onto the sample surface. As shown in Figure S4, the surface tension changes significantly with the concentration of the SDS. Upon introducing SDS into an aqueous solution, the surfactant partitions into the surface, reducing the surface tension by lowering the energy of the
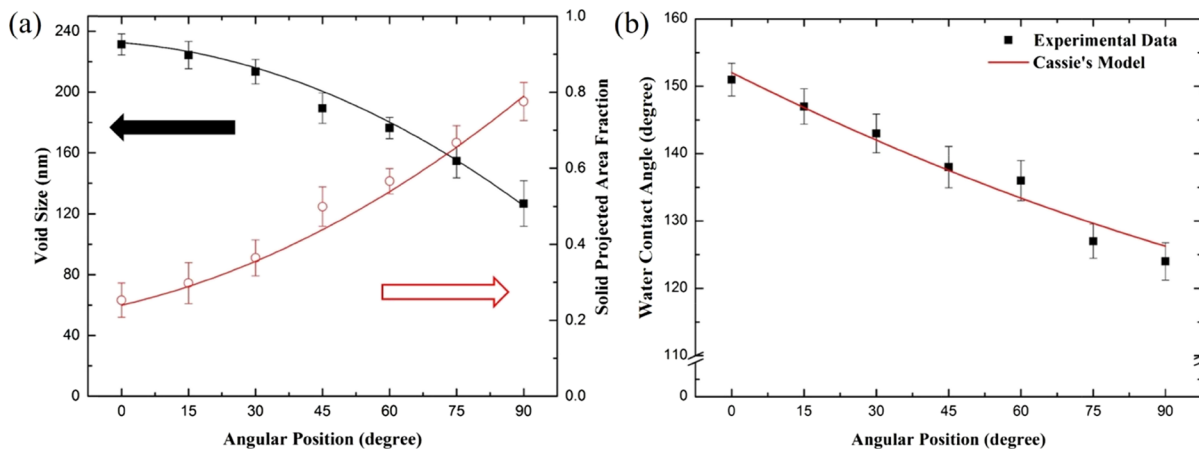

Figure 5. (a) Dependence of the void size and the corresponding projected area fraction on the angular position of curved macroporous photonic crystals after a 1 min plasma etching treatment. (b) Experimental and calculated SWCAs of the fluorosilane-modified curved macroporous photonic crystals at various angular positions.

surface. Subsequently, when the surface coverage by SDS increases, the surface tension decreases until the concentration reaches 0.5 wt %. Any further increase of SDS concentration does not affect the surface tension of the aqueous solution. Importantly, a clear tendency of the solution-infiltrated angular position with the concentration of SDS is observed (Figure 6).
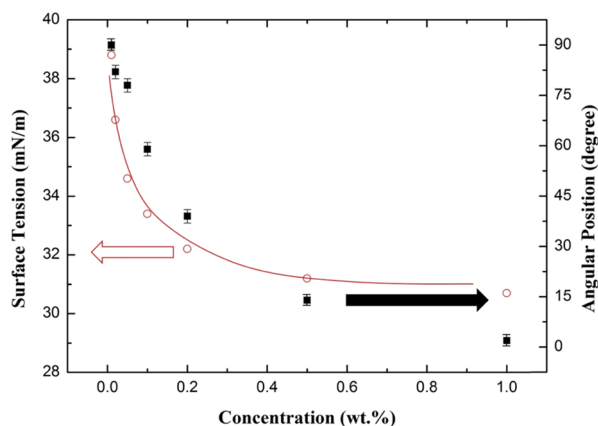

Figure 6. Dependence of the surface tension and the solution-infiltrated angular position on the concentration of aqueous SDS solutions.

The addition of a surfactant reduces the surface tension of an aqueous solution, allowing the solution to penetrate hydrophobic porous media. By comparing the experimental results, it is evident that a lower surface tension is associated with a smaller angular position. This suggests that the aqueous solution with higher surfactant concentration can infiltrate the angular position of macroporous photonic crystals with higher hydrophobicity. The methodology provides a detection range between 0.01 and 1 wt %, which covers the surfactant concentrations present in most industrial wastewater and municipal sewer discharges.[8] However, even though the detection range is compared fairly with previously reported detection technologies, it is not surprising that the minimum quantification limit of the photonic crystal-sensing materials for surfactants is less sensitive to the detection limits of other detection methods.[8−15,55−58]

A demonstration to verify the designed concepts is performed in Figure 7a. As a proof-of-concept, three drops of aqueous solution containing 0.2 wt % SDS are deposited onto the surface of fluorosilane-modified curved macroporous photonic crystals at 0°, 20°, and 40°. The formation of a spherical droplet at 0° (left droplet) and a hemispherical droplet at 20° (middle droplet) can be observed. In addition, the macroporous photonic crystals underneath the droplets display a shining blue color. In comparison with that, the solution penetrates the substrate right after a droplet of solution contacts the curved macroporous photonic crystals at 40° (right droplet). The filling of air cavities by an aqueous solution leads to a relatively high effective refractive index and a relatively small refractive index contrast of the medium. This further causes a red shift in the Bragg diffraction peak and decreased reflection amplitude (Figure 7b). The macroporous photonic crystals therefore exhibit a Kelly green color, caused by Bragg diffraction of incident white light, at 40°. Therefore, the use of curve macroporous photonic crystals provides instant visible readout during surfactant sensing. More importantly, the center of Kelly green spot can be located to determine the belonging angular position even if the solution droplet will span several angles. It is worth mentioning that the optical characteristics of the photonic crystals can be completely recovered after rinsing with ethanol and can thus be reused for surfactant detection.

For further understanding of surfactant detection capability, the as-fabricated curve macroporous photonic crystals are applied to detect aqueous solutions containing different concentrations of CTAB, a commonly used cationic surfactant, or hybrid surfactants (a 1:1 mixture of SDS with CTAB). In comparison with Figure 6, the results in Figures S5 and S6 reveal that the responses of CTAB detection and hybrid surfactants detection are similar with that of SDS detection. Although sensing performances of different surfactants cannot be distinguished, different types of surfactants can be detected by using the surface-modified curve macroporous photonic crystals.

4. CONCLUSIONS

In summary, a convenient and scalable doctor-blade-coating technology for fabricated three-dimensional curved macroporous photonic crystals with different hydrophobicities at
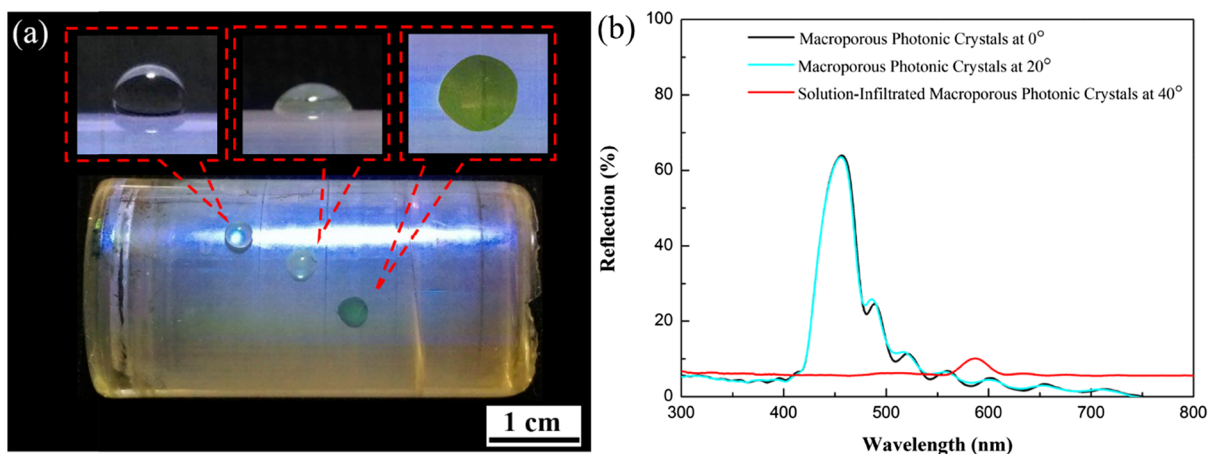

Figure 7. (a) Photograph of aqueous SDS solution (0.2 wt %) drops on fluorosilane-modified curved macroporous photonic crystals. (b) Normal incidence specular reflection spectra obtained from fluorosilane-modified curved macroporous photonic crystals and the sample that has been infiltrated with an aqueous SDS solution (0.2 wt %).

various angular positions is developed. An aqueous solution with higher surfactant concentration can penetrate the curved macroporous photonic crystals with higher hydrophobicity, leading to a color change at a smaller angular position. The as-fabricated photonic crystals not only offer an instant visible readout but also show promising sensitivity for aqueous solutions containing low concentration surfactants. It is believed that the methodology provides a platform for preparing portable chemical detectors for a variety of surfactants, which are promising for monitoring the concentration of surfactants released to environment.

ASSOCIATED CONTENT

Supporting Information

The Supporting Information is available free of charge on the ACS Publications website at DOI: 10.1021/acsami.7b06668.

Top-view SEM images of a curved 255 nm silica colloidal crystal−polymer composite fabricated by plasma etching for 1 min at 0°, cross-sectional SEM images of the curved macroporous photonic crystals fabricated by plasma etching a silica colloidal crystal−polymer composite for 1 min, followed by selective removal of the templating silica microspheres at various angular positions, photograph and reflection spectrum of curved macroporous photonic crystals templated from 255 nm silica microspheres (1 cm in diameter), dependence of the surface tension on the concentration of aqueous SDS solutions, dependence of the surface tension and the solution-infiltrated angular position on the concentration of aqueous CTAB solutions, and dependence of the surface tension and the solution-infiltrated angular position on the concentration of aqueous SDS/CTAB mixtures (PDF)

AUTHOR INFORMATION

Corresponding Authors
*E-mail: linky@dragon.nchu.edu.tw (K.-Y.A.L.).
*E-mail: hyang@dragon.nchu.edu.tw (H.Y.).

ORCID
Kun-Yi Andrew Lin: 0000-0003-1058-3097
Hongta Yang: 0000-0002-5822-1469

Notes
The authors declare no competing financial interest.

ACKNOWLEDGMENTS

REFERENCES

(1) Bhajanthri, N. K.; Arumugam, V. K.; Chokkareddy, R.; Redhi, G. G. Ionic Liquid Based High Performance Electrochemical Sensor for Ascorbic Acid in Various Foods and Pharmaceuticals. *J. Mol. Liq.* **2016**, *222*, 370−376.

(2) Hussain, S.; Malik, A. H.; Iyer, P. K. Highly Precise Detection, Discrimination, and Removal of Anionic Surfactants over the Full pH Range via Cationic Conjugated Polymer: An Efficient Strategy to Facilitate Illicit-Drug Analysis. *ACS Appl. Mater. Interfaces* **2015**, *7*, 3189−3198.

(3) Sanati, A. L.; Karimi-Maleh, H.; Badiei, A.; Biparva, P.; Ensafi, A. A. A Voltammetric Sensor Based on NiO/CNTs Ionic Liquid Carbon Paste Electrode for Determination of Morphine in the Presence of Diclofenac. *Mater. Sci. Eng., C* **2014**, *35*, 379−385.

(4) Huber, L.; Nitschke, L.; Holmberg, K. *Handbook of Applied Surface and Colloid Chemistry*; Wiley: Chichester, U.K., 2002; pp 509−536.

(5) Yuan, C. L.; Xu, Z. Z.; Fan, M. X.; Liu, H. Y.; Xie, Y. H.; Zhu, T. Study on Characteristics and Harm of Surfactants. *J. Chem. Pharm. Res.* **2014**, *6*, 2233−2237.

(6) Guzman, M. L.; Marques, M. R.; Olivera ME, M. E.; Stippler, E. S. Enzymatic Activity in the Presence of Surfactants Commonly Used in Dissolution Media, Part 1: Pepsin. *Results Pharma Sci.* **2016**, *6*, 15−19.

(7) Beltrán-Heredia, J.; Sánchez-Martín, J.; Solera-Hernández, C. Anionic Surfactants Removal by Natural Coagulant/Flocculant Products. *Ind. Eng. Chem. Res.* **2009**, *48*, 5085−5092.

(8) Zhang, J.-T.; Smith, N.; Asher, S. A. Two-Dimensional Photonic Crystal Surfactant Detection. *Anal. Chem.* **2012**, *84*, 6416−6420.

(9) Escrig-Doménech, A.; Simó-Alfonso, E. F.; Ramis-Ramos, G. Determination of the Four Major Surfactant Classes in Cleaning Products by Reversed-Phase Liquid Chromatography Using Serially Connected UV and Evaporative Light-Scattering Detection. *Anal. Chim. Acta* **2016**, *932*, 106−113.

(10) Olkowska, E.; Polkowska, Ż.; Namieśnik, J. Analytics of Surfactants in the Environment: Problems and Challenges. *Chem. Rev.* **2011**, *111*, 5667−5700.

(11) Hussain, S.; Malik, A. H.; Iyer, P. K. Highly Precise Detection, Discrimination, and Removal of Anionic Surfactants over the Full pH Range via Cationic Conjugated Polymer: An Efficient Strategy to Facilitate Illicit-Drug Analysis. *ACS Appl. Mater. Interfaces* **2015**, *7*, 3189−3198.

(12) Escrig-Doménech, A.; Simó-Alfonso, E. F.; Herrero-Martínez, J. M.; Ramis-Ramos, G. Derivatization of Hydroxyl Functional Groups for Liquid Chromatography and Capillary Electroseparation. *J. Chromatogr. A* **2013**, *1296*, 140−156.

(13) Takahashi, K.; Kinugasa, S.; Senda, M.; Kimizuka, K.; Fukushima, K.; Matsumoto, T.; Shibata, Y.; Christensen, J. Quantitative Comparison of a Corona-Charged Aerosol Detector and an Evaporative Light-Scattering Detector for the Analysis of a Synthetic Polymer by Supercritical Fluid Chromatography. *J. Chromatogr. A* **2008**, *1193*, 151−155.

(14) Ripoll-Seguer, L.; Beneito-Cambra, M.; Herrero-Martínez, J. M.; Simó-Alfonso, E. F.; Ramis-Ramos, G. Determination of Non-Ionic and Anionic Surfactants in Industrial Products by Separation on a Weak Ion-Exchanger, Derivatization and Liquid Chromatography. *J. Chromatogr. A* **2013**, *1320*, 66−71.

(15) Norton, D.; Shamsi, S. A. Capillary Electrochromatography−Mass Spectrometry of Nonionic Surfactants. *Anal. Chem.* **2007**, *79*, 9459−9470.

(16) Härmä, H.; Laakso, S.; Pihlasalo, S.; Hänninen, P.; Faure, B.; Rana, S.; Bergström, L. Rapid Detection of Trace Amounts of Surfactants Using Nanoparticles in Fluorometric Assays. *Nanoscale* **2010**, *2*, 69−71.

(17) Joannopoulos, J. D.; Meade, R. D.; Winn, J. N. *Photonic Crystals*; Princeton University Press: Princeton, 1995.

(18) Ryu, S. H.; Gim, M.-J.; Lee, W.; Choi, S.-W.; Yoon, D. K. Switchable Photonic Crystals Using One-Dimensional Confined Liquid Crystals for Photonic Device Application. *ACS Appl. Mater. Interfaces* **2017**, *9*, 3186−3191.

(19) Potyrailo, R. A.; Ghiradella, H.; Vertiatchikh, A.; Dovidenko, K.; Cournoyer, J. R.; Olson, E. Morpho Butterfly Wing Scales Demonstrate Highly Selective Vapour Response. *Nat. Photonics* **2007**, *1*, 123−128.

(20) Tsao, K.-Y.; Tsai, H.-P.; Lin, K.-Y. A.; He, Y.-X.; Yang, H. Self-Assembled Hierarchical Arrays for Colored Retroreflective Coatings. *Langmuir* **2016**, *32*, 12869−12875.

(21) Ko, Y.-L.; Tsai, H.-P.; Lin, K.-Y.; Chen, Y.-C.; Yang, H. Reusable Macroporous Photonic Crystal-Based Ethanol Vapor Detectors by Doctor Blade Coating. *J. Colloid Interface Sci.* **2017**, *487*, 360−369.

(22) Zhang, Y.; Li, X.; Gao, L.; Qiu, J.; Heng, L.; Tang, B. Z.; Jiang, L. Silole-Infiltrated Photonic Crystal Films as Effective Fluorescence Sensor for Fe^{3+} and Hg^{2+}. *ChemPhysChem* **2014**, *15*, 507−513.

(23) Zhang, Y.; Qiu, J.; Gao, M.; Li, P.; Gao, L.; Heng, L.; Tang, B. Z.; Jiang, L. A Visual Film Sensor Based on Silole-Infiltrated SiO_2 Inverse Opal Photonic Crystal for Detecting Organic Vapors. *J. Mater. Chem. C* **2014**, *2*, 8865−8872.

(24) Zhang, Y.; Qiu, J.; Hu, R.; Li, P.; Gao, L.; Heng, L.; Tang, B. Z.; Jiang, L. A Visual and Organic Vapor Sensitive Photonic Crystal Sensor Consisting of Polymer-Infiltrated SiO_2 Inverse Opal. *Phys. Chem. Chem. Phys.* **2015**, *17*, 9651−9658.

(25) Zhang, Y.; Mu, L.; Zhou, R.; Li, P.; Liu, J.; Gao, L.; Heng, L.; Jiang, L. Fluoral-p Infiltrated SiO_2 Inverse Opal Photonic Crystals as Fluorescent Film Sensors for Detecting Formaldehyde Vapor. *J. Mater. Chem. C* **2016**, *4*, 9841−9847.

(26) Huang, L.; Tian, H.; Zhou, J.; Liu, Q.; Zhang, P.; Ji, Y. Label-Free Optical Sensor by Designing a High-Q Photonic Crystal Ring−Slot Structure. *Opt. Commun.* **2015**, *335*, 73−77.

(27) Zhao, Y.; Xie, Z.; Gu, H.; Zhu, C.; Gu, Z. Bio-Inspired Variable Structural Color Materials. *Chem. Soc. Rev.* **2012**, *41*, 3297−3317.

(28) Chou, S. Y.; Keimel, C.; Gu, J. Ultrafast and Direct Imprint of Nanostructures in Silicon. *Nature* **2002**, *417*, 835−837.

(29) Rolland, J. P.; Maynor, B. W.; Euliss, L. E.; Exner, A. E.; Denison, G. M.; Desimone, J. M. Direct Fabrication and Harvesting of Monodisperse, Shape-Specific Nanobiomaterials. *J. Am. Chem. Soc.* **2005**, *127*, 10096−10100.

(30) Lee, M. H.; Huntington, M. D.; Zhou, W.; Yang, J.-C.; Odom, T. W. Programmable Soft Lithography: Solvent-Assisted Nanoscale Embossing. *Nano Lett.* **2011**, *11*, 311−315.

(31) Kim, S.-H.; Park, Y. S.; Choi, J. H.; Shim, J. W.; Yang, S.-M. Integration of Colloidal Photonic Crystals toward Miniaturized Spectrometers. *Adv. Mater.* **2010**, *22*, 946−950.

(32) Zhao, Y.; Xie, Z.; Gu, H.; Jin, L.; Zhao, X.; Wang, B.; Gu, Z. Multifunctional Photonic Crystal Barcodes from Microfluidics. *NPG Asia Mater.* **2012**, *4*, No. e25.

(33) Chen, Y. Nanofabrication by Electron Beam Lithography and Its Applications: A Review. *Microelectron. Eng.* **2015**, *135*, 57−72.

(34) Liu, G.; Zhou, L.; Wang, C.; Wu, Y.; Li, Y.; Fan, Q.; Shao, J. Study on the High Hydrophobicity and Its Possible Mechanism of Textile Fabric with Structural Colors of Three-Dimensional Poly-(Styrene-Methacrylic Acid) Photonic Crystals. *RSC Adv.* **2015**, *5*, 62855−62863.

(35) Sabapathy, M.; Pushpam, S. D. C.; Basavaraj, M. G.; Mani, E. Synthesis of Single and Multipatch Particles by Dip-Coating Method and Self-Assembly Thereof. *Langmuir* **2015**, *31*, 1255−1261.

(36) Mine, E.; Hirose, M.; Nagao, D.; Kobayashi, Y.; Konno, M. Synthesis of Submicrometer-Sized Titania Spherical Particles with a Sol−Gel Method and Their Application to Colloidal Photonic Crystals. *J. Colloid Interface Sci.* **2005**, *291*, 162−168.

(37) Xiao, P.; Gu, J.; Wan, C.; Wang, S.; He, J.; Zhang, J.; Huang, Y.; Kuo, S.-W.; Chen, T. Ultrafast Formation of Free-Standing 2D Carbon Nanotube Thin Films through Capillary Force Driving Compression on an Air/Water Interface. *Chem. Mater.* **2016**, *28*, 7125−7133.

(38) Kong, X.; Xi, Y.; LeDuff, P.; Li, E.; Liu, Y.; Cheng, L.-J.; Rorrer, G. L.; Tan, H.; Wang, A. X. Optofluidic Sensing from Inkjet-Printed Droplets: The Enormous Enhancement by Evaporation-Induced Spontaneous Flow on Photonic Crystal Biosilica. *Nanoscale* **2016**, *8*, 17285−17294.

(39) Askar, K.; Leo, S.-Y.; Xu, C.; Liu, D.; Jiang, P. Rapid Electrostatics-Assisted Layer-by-Layer Assembly of Near-Infrared-Active Colloidal Photonic Crystals. *J. Colloid Interface Sci.* **2016**, *482*, 89−94.

(40) Lin, C.-Y.; Lin, K.-Y.; Tsai, H.-P.; He, Y.-X.; Yang, H. Self-Assembled Dual-Sided Hemispherical Nano-Dimple-Structured Broadband Antireflection Coatings. *Appl. Phys. Lett.* **2016**, *109*, 221601.

(41) Yang, H.; Jiang, P. Large-Scale Colloidal Self-Assembly by Doctor Blade Coating. *Langmuir* **2010**, *26*, 13173−13182.

(42) Cai, C.-Y.; Lin, K.-Y. A.; Chen, Y.-C.; Yang, H. Macroporous Photonic Crystal-Based Anti-Ultraviolet and Anti-Near-Infrared Materials by Doctor Blade Coating. *Appl. Phys. Lett.* **2016**, *108*, 071906.

(43) Yang, H.; Jiang, P. Macroporous Photonic Crystal-Based Vapor Detectors Created by Doctor Blade Coating. *Appl. Phys. Lett.* **2011**, *98*, 011104.

(44) Nakamura, T.; Yamada, Y.; Yamada, H.; Yano, K. A Novel Route to Luminescent Opals for Controlling Spontaneous Emission. *J. Mater. Chem.* **2009**, *19*, 6699−6705.

(45) Bai, L.; Xie, Z.; Cao, K.; Zhao, Y.; Xu, H.; Zhu, C.; Mu, Z.; Zhong, Q.; Gu, Z. Hybrid Mesoporous Colloid Photonic Crystal Array for High Performance Vapor Sensing. *Nanoscale* **2014**, *6*, 5680−5685.

(46) Park, S.-G.; Moon, H. H.; Lee, S.-K.; Shim, J.; Yang, S.-M. Bioinspired Holographically Featured Superhydrophobic and Super-sticky Nanostructured Materials. *Langmuir* **2010**, *26*, 1468−1472.

(47) Cai, C.-Y.; Lin, K.-Y. A.; Yang, H. Superhydrophobic Anti-Ultraviolet Films by Doctor Blade Coating. *Appl. Phys. Lett.* **2014**, *105*, 201913.

(48) Dutschk, V.; Sabbatovskiy, K. G.; Stolz, M.; Grundke, K.; Rudoy, V. M. Unusual Wetting Dynamics of Aqueous Surfactant Solutions on Polymer Surfaces. *J. Colloid Interface Sci.* **2003**, *267*, 456−462.

(49) Ivanova, N.; Starov, V.; Johnson, D.; Hilal, N.; Rubio, R. Spreading of Aqueous Solutions of Trisiloxanes and Conventional Surfactants over PTFE AF Coated Silicone Wafers. *Langmuir* **2009**, *25*, 3564−3570.

(50) Ivanova, N. A.; Xhantenova, Z. B.; Starov, V. M. Wetting Dynamics of Polyoxyethylene Alkyl Ethers and Trisiloxanes in Respect of Polyoxyethylene Chains and Properties of Substrates. *Colloids Surf., A* **2012**, *413*, 307−313.

(51) Stöber, W.; Fink, A.; Bohn, E. Controlled Growth of Monodisperse Silica Spheres in the Micron Size Range. *J. Colloid Interface Sci.* **1968**, *26*, 62−69.

(52) Plueddemann, E. P. *Silane Coupling Agents*, 2nd ed.; Plenum Press: New York, 1991.

(53) Satake, M.; Iwase, T.; Kurihara, M.; Negishi, N.; Tada, Y.; Yoshida, H. Effect of Oxygen Addition to an Argon Plasma on Etching Selectivity of Poly(Methyl Methacrylate) to Polystyrene. *J. Micro/Nanolithogr., MEMS, MOEMS* **2013**, *12*, 041309.

(54) Jiang, P.; Bertone, J. F.; Hwang, K. S.; Colvin, V. L. Single-Crystal Colloidal Multilayers of Controlled Thickness. *Chem. Mater.* **1999**, *11*, 2132−2140.

(55) Levine, L. H.; Garland, J. L.; Johnson, J. V. HPLC/ESI-Quadrupole Ion Trap Mass Spectrometry for Characterization and Direct Quantification of Amphoteric and Nonionic Surfactants in Aqueous Samples. *Anal. Chem.* **2002**, *74*, 2064−2071.

(56) Radke, M.; Behrends, T.; Förster, J.; Herrmann, R. Analysis of Cationic Surfactants by Microbore High-Performance Liquid Chromatography−Electrospray Mass Spectrometry. *Anal. Chem.* **1999**, *71*, 5362−5366.

(57) Kamaya, M.; Sugimoto, H.; Yamaguchi, Y. A Simple and Rapid Method for the Detection of Non-Ionic Surfactants. *Am. J. Anal. Chem.* **2014**, *05*, 1121−1128.

(58) Härmä, H.; Laakso, S.; Pihlasalo, S.; Hänninen, P.; Faure, B.; Rana, S.; Bergström, L. Rapid Detection of Trace Amounts of Surfactants using Nanoparticles in Fluorometric Assays. *Nanoscale* **2010**, *2*, 69−71.